SAND2016-6413C
Proceedings of DSCC 2016
ASME 2016 Dynamic Systems and Controls Conference
October 24-28, 2016, Minneapolis, USA

DSCC2016-9738

IMPROVING ROBOTIC ACTUATOR TORQUE DENSITY AND EFFICIENCY THROUGH ENHANCED HEAT TRANSFER

Anirban Mazumdar
Steven J. Spencer
Clinton Hobart
Michael Kuehl
Gregory Brunson
Nadia Coleman
Stephen P. Buerger
High Consequence Automation and Robotics
Sandia National Laboratories
Albuquerque, New Mexico, 87123
Email: amazumd@sandia.gov

ABSTRACT

Electric motors are a popular choice for mobile robots because they can provide high peak efficiencies, high speeds, and quiet operation. However, the continuous torque performance of these actuators is thermally limited due to joule heating, which can ultimately cause insulation breakdown. In this work we illustrate how motor housing design and active cooling can be used significantly improve the ability of the motor to transfer heat to the environment. This can increase continuous torque density and reduce energy consumption. We present a novel housing design for brushless DC motors that provides improved heat transfer. This design achieves a 50% *increase in heat transfer over a nominal design. Additionally, forced air or water cooling can be easily added to this configuration. Forced convection increases heat transfer over the nominal design by* 79% *with forced air and* 107% *with pumped water. Finally, we show how increased heat transfer reduces power consumption and we demonstrate that strategically spending energy on cooling can provide net energy savings of* $4\% - 6\%$. [1] [2]

NOMENCLATURE

R_{coil} Motor phase resistance, (Ω).
I Motor current, (A).
I_{max} Maximum continuous motor current, (A).
α Temperature coefficient of resistance for copper, ($0.0039/K$).
K_m Motor constant, ($Nm/\sqrt{W}$).
K_t Torque sensitivity, (Nm/A).
τ Motor torque, (Nm).
R_0 Nominal phase resistance at T_0, (Ω).
Q_d Power dissipated by motor phases, (W).
Q_s Power saved by active cooling, (W).

[1] Sandia National Laboratories is a multi-program laboratory managed and operated by Sandia Corporation, a wholly owned subsidiary of Lockheed Martin Corporation, for the U.S. Department of Energy's National Nuclear Security Administration under contract DE-AC04-94AL85000.

[2] The United States Government retains, and by accepting the article for publication, the publisher acknowledges that the United States Government retains, a non-exclusive, paid-up, irrevocable, worldwide license to publish or reproduce the published form of this work, or allow others to do so, for United States Government purposes.

Q_{fan} Power used to drive cooling fans, (W).
T_0 Nominal temperature, $(^\circ C)$.
T_a Ambient temperature, $(^\circ C)$.
T_{coil} Ambient temperature, $(^\circ C)$.
T_I Back iron surface temperature, $(^\circ C)$.
T_{max} Maximum coil temperature, $(^\circ C)$.
H_m Motor heat transfer coefficient, (W/K).
r_1 Thermal resistance of coil-to-iron path, (K/W).
r_2 Thermal resistance of iron-to-environment path, (K/W).
r_{coil} Thermal resistance of the motor coils, (K/W).
r_{ins} Thermal resistance of the outer insulation, (K/W).
$r_{gap,t}$ Thermal resistance of the top air gap, (K/W).
$r_{gap,b}$ Thermal resistance of the bottom air gap, (K/W).
r_{iron} Thermal resistance of the back iron, (K/W).
$r_{housing}$ Thermal resistance of the aluminum motor housing, (K/W).
r_{env} Thermal resistance of between the motor surface and the environment, (K/W).

INTRODUCTION

The use of electric motors is common in robotic applications due to their relatively high peak efficiencies, high speeds, and quiet operation. However, one important drawback with electric motors is their relatively low continuous torque density [1, 2]. Torque limitations are problematic for mobile robots that must carry their own actuators, and robot failures due to overheating are not uncommon. The continuous performance of electric motors is thermally limited, with the thermal breakdown of insulation generally occurring near $130^\circ C$. Insulation with higher breakdown temperatures can be found, but demagnetization of permanent magnets can also occur at elevated temperatures.

Energy dissipation in electric motors is proportional to the square of motor torque, so thermal limitations place an upper limit on the continuous torque performance. Increasing motor heat transfer has therefore emerged as an important research area for mobile robotic applications [3–8]. Improved heat dissipation can provide increased continuous torque and higher torque density, thereby enabling smaller actuators.

Additionally, good heat transfer can also improve efficiency by keeping the temperature of the motor windings low (thereby reducing their resistance). Energy efficiency is very important in mobile robots because they carry their own power supply. Motors dissipate more energy per unit current when their temperature increases. Therefore, ensuring that motors remain cool can improve overall system level efficiency. This can be achieved through housing design and through the addition of active cooling elements.

In this work, we present a novel housing design for frameless brush-less DC motors that provides improved heat transfer over nominal designs. The work in this paper focuses on relatively small changes to the motor topology and the addition of simple components. This design only involves adjustments to the motor housing structure and not the motor coils or back iron, enabling broad applicability. In this regard, our methods are similar to those described in [4–6] which focused on relatively simple modifications to motors. However, the cooling technique in [6] relies on the evaporation of a fixed quantity of liquid water, and the systems used in [4, 5] exploit centrally located liquid cooling infrastructure which is used to cool multiple motors. Our approach also differs from the more specific approaches described in [3, 7, 8] which achieve excellent torque density by incorporating heat transfer analysis and cooling elements into the design of the motor stators and coils.

The open framed design shown in Fig. 1, provides a 50% increase in heat transfer over a nominal design without the additional weight of metal fins. In addition, active forced air or forced liquid cooling can be easily combined with this design. Forced air cooling provides an 79% increase in heat transfer over the nominal design, with minimal size and mass penalties. A liquid cooling jacket can be placed around the exposed stator of the motor to provide forced liquid cooling. While liquid cooling requires additional hardware (pump, radiator, tubing), it provides a 107% increase in heat transfer over the nominal design. By reducing the temperature of the motor windings, these designs also reduce motor power consumption. We show how the reduction in motor power can even exceed the power required for forced cooling (to power fan or pump). Experimental data illustrates this net energy "win."

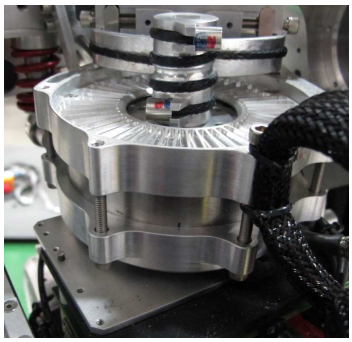

Figure 1. A PHOTOGRAPH ILLUSTRATING THE OPEN-FRAMED MOTOR DESIGN

This paper begins by describing an overall system model that relates electromechanical performance to thermal conditions. We then use this model to motivate our unique motor frame design and describe the features of our design in detail. Experimental results are used to illustrate the performance of this system with various configurations including forced air and liquid cooling. Comparisons with the nominal specifications as well as a basic motor housing design are used to demonstrate the

efficacy of our approach.

SYSTEM OVERVIEW

System Model

Heat in motors can be generated from a variety of sources including friction in the bearings, eddy current effects, and joule heating in the windings. In this work, our analysis focuses on electrical power power dissipation caused by joule heating, Q_d.

$$Q_d = I^2 R_{coil} \tag{1}$$

The coil resistance depends on the temperature change of the coil and the temperature coefficient of resistivity, α.

$$R_{coil} = R_0(1+\alpha(T_{coil}-T_0)) \tag{2}$$

The temperature increase of the coils can be modeled using a lumped heat transfer coefficient, H_m. H_m represents the combination of all the thermal resistances between the copper coils and the ambient air surrounding the motor.

$$Q_d = H_m(T_{coil}-T_a) \tag{3}$$

These expressions can be combined to compute the steady state temperature of the coil, T_{coil}, and the amount of electrical power dissipated in the motor windings, Q_d, as a function of the continuous motor current, I.

$$T_{coil} = \frac{I^2 R_0 (1-\alpha T_0) + H_m T_a}{H_m - I^2 R_0 \alpha} \tag{4}$$

$$Q_d = I^2 R_0 \left(1+\alpha\left(\frac{I^2 R_0 (1-\alpha T_0) + H_m T_a}{H_m - I^2 R_0 \alpha} - T_0\right)\right) \tag{5}$$

One of the most important operating conditions is predicting how improved heat transfer enables increased currents. We can use Eqn. 4 to determine the maximum current, I_{max} based on the breakdown temperature of the coils, T_{max}. This results in the following expression.

$$I_{max} = \sqrt{\frac{(T_{max}-T_a)H_m}{R_0(1+\alpha(T_{max}-T_0))}} \tag{6}$$

This expression illustrates that given a fixed ambient temperature, T_a, the maximum current, I_{max}, scales with square root of the heat transfer coefficient, H_m.

Nominal Motor Design

The motor designs described in this work are based around the Allied Motion Megaflux Series frameless 3-phase brushless DC motors. These motors were chosen for their high continuous and peak torques. This enables minimal transmission ratios, enabling high efficiency and quality torque control at the joints.

The use of a frameless design enables a high degree of design freedom for the motor housing. A rendering of an unframed motor is shown in Fig. 2-a, and photos of an unhoused stator and rotor are shown in Fig. 2-b.

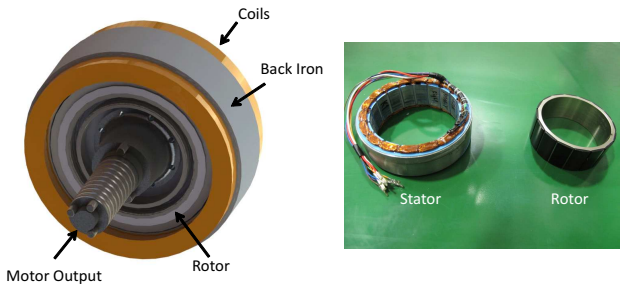

(A) Frameless Motor Rendering (B) Frameless Motor Components

Figure 2. A RENDERING OF THE MOTOR CONFIGURATION (A) AND A PHOTO OF THE FRAMELESS MOTOR COMPONENTS (B).

For the scope of this work we examine the performance of the MF0127032-X0X. Baseline performance metrics are provided by the manufacturer based on the assumption that the motor is placed in still air and mounted to an aluminum heat sink. The baseline heat transfer coefficient is estimated by the manufacturer to be $1.01 W/K$. The breakdown temperature for the laminations is $130^{\circ}C$. The rated continuous stall torque and stall current are $6.55 Nm$ and $7.34 A$ respectively. The nominal resistance was measured to be $R_0 = 1.48\Omega$, at a nominal temperature $T_0 = 21^{\circ}C$.

Simplified Heat Transfer Model

To develop a greater understanding of the heat transfer, we consider a very simple housing design (assumed to be aluminum) that covers the stator and holds it in place. We assume that the heat transfer occurs primarily through 3 paths: radially outward from the wires into the back iron, upwards from the coils to the case, and downwards from the coils to the case. As Fig. 3 shows, we treat the windings/insulation as cylinders that point in and out of the page. We also assume an air gap between the top/bottom of the coils and the housing.

A resistor network representation is shown in Fig. 4. This model appropriate for examining the relative size of the thermal resistances, and identifying the bottlenecks to heat transfer.

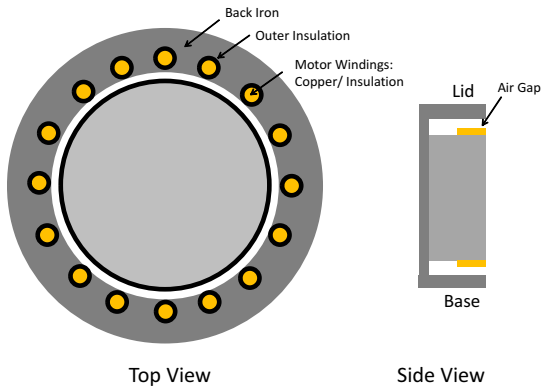

Figure 3. ILLUSTRATIONS OF THE SIMPLIFIED HEAT TRANSFER MODEL.

The radial path represents the heat flow out to the environment through the sides of the motor. The term r_{coil} is used to model the conduction through the sets of coils. Estimating this heat transfer is challenging due to the complex network of copper, insulation, and air gaps. A bulk thermal conductivity can be used as outlined in [3]. The term r_{ins} is used to model the conduction from the windings through the outer insulation. The heat is then conducted through the back iron, r_{iron}, to the housing.

The top and bottom heat transfer paths are nearly identical to each other. In this case there is no outer insulation, and the heat flows directly from the coils into the air gap. The terms $r_{gap,t}$ and $r_{gap,b}$ represent the thermal conduction through the air gap to the housing for the top and bottom respectively.

Heat is transferred through the housing to the outer surfaces of the motor. Heat flows from the outer surfaces to the environment via free convection (in the absence of fans or pumps). The term r_{env} is used to represent the thermal resistance between the motor surface and the environment.

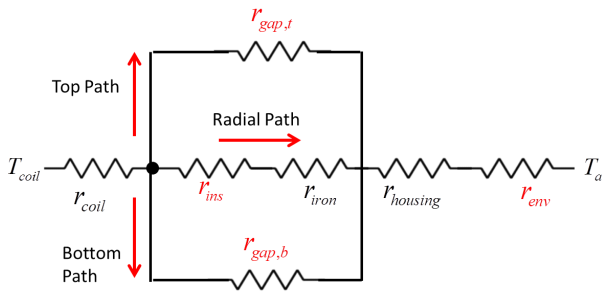

Figure 4. THE RESISTOR NETWORK USED TO APPROXIMATE MOTOR HEAT TRANSFER.

Analysis of the heat transfer parameters reveals that $r_{gap,t}$, $r_{gap,b}$, r_{ins}, and r_{env} are all on the order of $1K/W$ or larger. These resistances, labeled in red in Fig. 4, are the main barriers to improved performance. Significant reductions to the thermal resistance between the housing and the environment, r_{env}, can be achieved through the use of forced air or water. The resistance, $r_{gap,t}$, can also be reduced by eliminating the air gap between the coils and the housing. In the following sections we attempt to increase performance by reducing $r_{gap,t}$, and r_{env}.

Experimental Procedure

Tests of the thermal properties of the motor designs were performed at Sandia National Laboratories. A current load was provided by applying a DC voltage across two of the motor phases. The lack of commutation causes the motor to stall, enabling testing of high current loads without physically locking the rotor. The dissipated electrical power, Q_d, is determined by measuring the input voltage and current to the motor.

Estimating temperature is challenging due to the high packing density of the motor coils. The motor is equipped with a thermistor, but this only provides the temperature at a specific location. For bulk heat transfer analysis we seek an average coil temperature estimate instead. We estimate this temperature using the resistance of the coil [9]. The expression in Eqn. 2 can be used to compute the average coil temperature based on the change in resistance.

This approach for estimating coil temperature based on the resistance was validated using a set of simple experiments. A frameless motor stator was placed in an oven with roughly uniform temperature. The system was allowed to sit for several hours to allow the temperature to stabilize. The temperature predicted by the thermistor is plotted against the prediction from the coil resistance. As Fig. 5 shows, coil resistance is an effective predictor of average coil temperature.

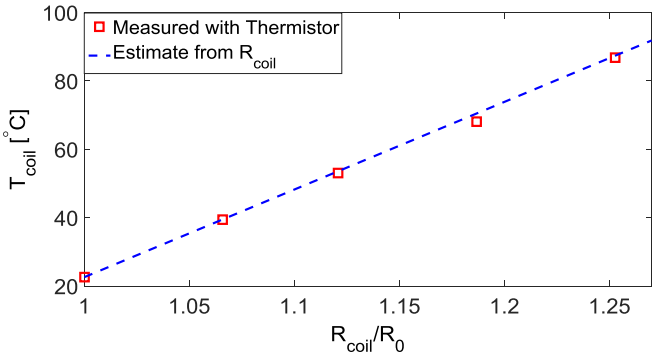

Figure 5. EXPERIMENTAL DATA SHOWING HOW RESISTANCE IS USED TO ESTIMATE COIL TEMPERATURE.

BASIC MOTOR PERFORMANCE

A design we termed the "basic housing design" is shown in Fig. 6. This design uses fins machined into the aluminum housing to enhance radial heat transfer from the coils to the environment. The aspect ratio and spacing of the fins were chosen to balance between size constraints, good performance, and ease of manufacturing. The predicted heat transfer paths are through the top and bottom of the coils and radially outward. We assume minimal heat transfer occurs radially inward due to the air gap and the presence of the rotor. The sample housing design illustrates some of the constraints on housing design. The lid and base are used to clamp the stator in place in order to prevent it from rotating and to prevent debris from entering the motor.

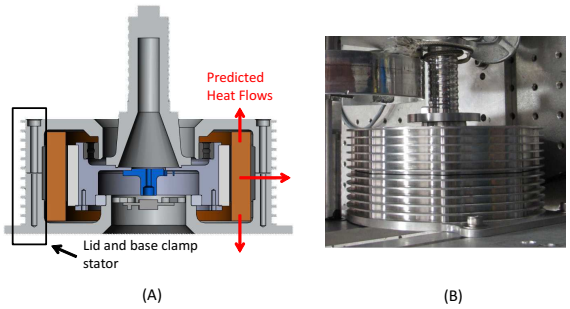

Figure 6. A RENDERING (A) AND PHOTOGRAPH (B) OF THE BASIC MOTOR HOUSING DESIGN.

Motor Performance, Passively Cooled

Stall current tests were performed at various levels to measure the heat transfer performance of the basic design. Currents ranging from $5A - 6.9A$ were applied. The ambient temperature of the room ranged from $21 - 23°C$. The heat transfer coefficient, H_m, was estimated using the expression in Eqn. 3. The results are shown in red in Fig. 7. As these results show, a single heat transfer coefficient of $1.25W/K$ fits the data well. This represents a 24% improvement over the nominal motor design.

Motor Performance, Forced Air Convection

To maximize the performance of the cooling fins, PC-style cooling fans were used to provide forced air-flow across the circumference of the motor housing. Two fans ($\sim 0.11kg$ total mass, 3% of motor mass) rated for flow rates of $0.014m^3/s$ were placed near the motor, and used to blow air over the motor housing. The fans consumed a combined power of $4.2W$. Again, stall current tests were performed, in this case with currents ranging from $5 - 7.9A$. The results are shown in blue in Fig. 7. As these results show, a single heat transfer coefficient of $1.77W/K$ fits

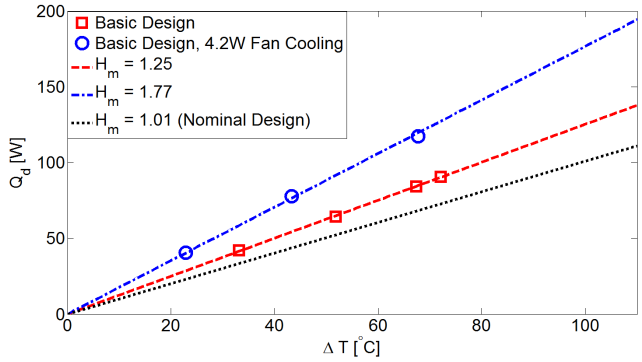

Figure 7. EXPERIMENTAL DATA FOR THE BASIC MOTOR'S HEAT TRANSFER PERFORMANCE.

the data. This is a 42% improvement over the passively cooled case, and a 75% improvement over the nominal motor design. Note how the $7.9A$ current load exceeds the specified current rating by 8%, but the coil temperature is only $91°C$. This illustrates how improved cooling can improve the torque output of these actuators. The 77% improvement in the heat transfer coefficient means that the continuous stall current rating should increase by 33%, from $7.3A$ to $9.7A$. The stall torque similarly increases from $6.55Nm$ to $8.7Nm$. The addition of active cooling increases the continuous torque density of the basic motor design by 15%.

Variable Forced Air

An experiment was performed to assess the role of cooling power on heat transfer performance. A fixed current command of $6.7A$ was used, and various levels of fan power were used ranging from $1.4W$ (near minimum power to operate fans) and $4.2W$ (full power). As Fig. 8-A illustrates, the initiation of forced air over the fins provides the bulk of the heat transfer benefit. Further increasing the fan power only marginally increases the heat transfer.

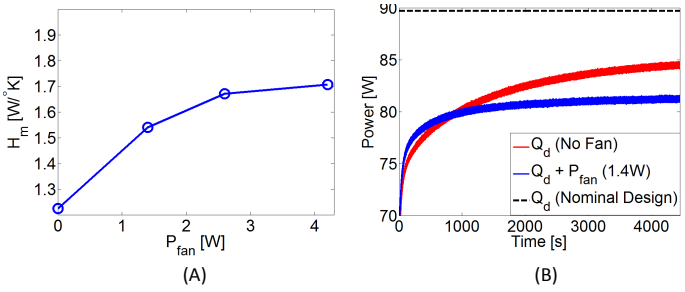

Figure 8. EXPERIMENTAL DATA ILLUSTRATING HEAT TRANSFER (A) AND POWER SAVINGS (B) FROM FORCED AIR CONVECTION.

Energetic Benefits

While small cooling fans provide substantial improvements to heat transfer, and only slightly increase net mass ($0.11kg$), they do consume additional power. Interestingly, we have found that by reducing the electrical resistance of the coils, R_{coils}, the fans can pay for themselves energy-wise and can even provide a clear net energy benefit. For example, Fig.8-B compares the electrical power dissipated in the motor, Q_d, when a $6.7A$ continuous stall current is applied. As the results demonstrate, the use of $1.4W$ of fan cooling power actually provides *net power savings* of at least $3.3W$ at steady state. In addition, when compared with the nominal motor design, our basic housing design combined with fan cooling enables projected energy savings of $7.7W$, or 9%.

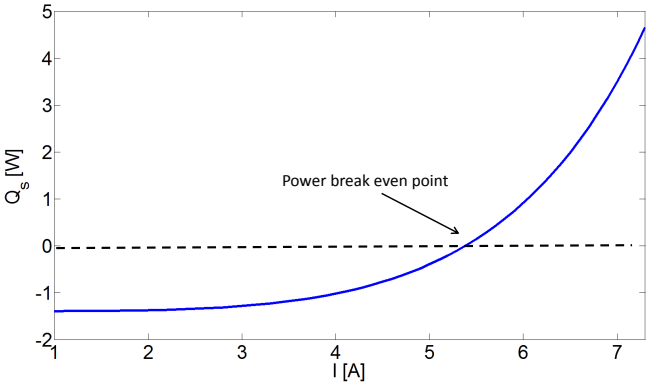

Figure 9. SIMULATION DATA ILLUSTRATING THE ENERGETIC BENEFITS FROM ACTIVE COOLING AT VARIOUS CURRENT LOADS.

Energy costs and savings from active cooling are load dependent. As we have shown, when there are large currents, active cooling can provide a "net win" by reducing the temperature of the windings. However, with smaller currents the motor windings dissipate less power and require less cooling. The energetic impact of cooling can be examined using the model in Eqn. 5. We compare the predicted power dissipation for the basic housing design with and without active cooling ($1.4W$) for a range of current levels. We use the variable, Q_s, to represent the power savings from active cooling.

$$Q_s = Q_d(I, Q_{fan} = 0) - Q_d(I, Q_{fan} = 1.4) - Q_{fan} \qquad (7)$$

The simulated results are shown in Fig. 9. These results illustrate that the energetic "break even" point for this motor is $I = 5.4A$. Above these current loads, the fans provide a net energy benefit. Below this load, the fans still improve heat transfer but cost net energy.

ENHANCED HEAT TRANSFER DESIGN

Based on the promising results with the basic motor design, we developed a second motor design intended to provide further improvements in heat transfer as well as reduced weight. The new design saves $\sim 0.3kg$ per motor by removing the fins. This design consists of two key changes to the design: the exposed stator and the flexible aluminum insert.

Exposed Stator

Heat is transferred radially outward from the coils into the back iron. The back-iron on the outside of the stator provides a good heat transfer path with a relatively low thermal resistance. The challenge is transferring heat from the back iron to the environment. The back iron layer is too thin to machine long fins, and altering the back iron risks altering the motor magnetic properties. While coupling fins to the back-iron layer was shown to provide improved performance, ensuring good contact between the back-iron and the aluminum fins is challenging. Heat transfer pastes can be used ensure contact but these are only designed for very small gaps and have thermal conductivities that are typically 1-2 orders of magnitude less than metals [10].

We enhance radial heat transfer by using an open-framed design that exposes the back-iron. As. Fig. 10-A shows, this reduces the motor housing mass and allows the back-iron to have a direct heat transfer path to the environment. In addition, we have designed the open-framed housing to accommodate an optional liquid cooling jacket. This jacket, shown in Fig. 10-B allows liquid to be pumped around the motor stator, greatly increasing heat transfer.

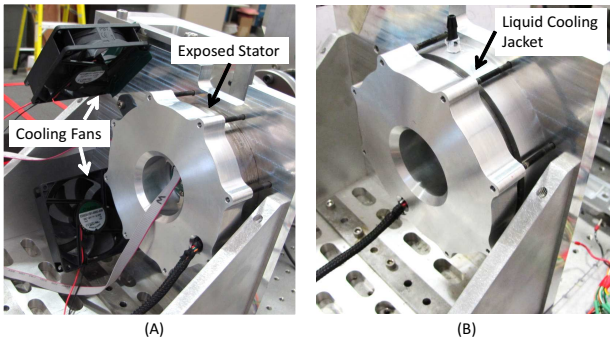

Figure 10. PHOTOGRAPHS OF THE EXPOSED STATOR (A) AND LIQUID COOLING JACKET (B).

Flexible Aluminum Insert

The tops of the coils also provide a heat transfer path to the environment. We speculate that because of the relatively short

coil height of these motors, the heat transfer through the end turns is larger than in other motor configurations. On these flat, large diameter motors, the end turns comprise a greater fraction of the exposed surface area than in other motor geometries such as tall, narrow designs.

The basic motor design described previously did not exploit this feature, with an air gap existing between the tops of the coils and the lid. To enhance the heat transfer to the lid we added a flexible aluminum ring designed to match the width of the coils. The lid then sits on top of this ring, creating a strong heat conduction path. Since the coils are not of uniform height, notches were machined into the ring, making it flexible and allowing it to conform to the coil shape. A photograph illustrating the aluminum insert with its notches is shown in Fig. 11-A. A photograph of the motor with the lid removed is shown in Fig. 11-B. The lid itself is designed to be thin and has fin-like surfaces machined into it (as in Fig.1). Compliance in both the ring and the lid ensures good thermal contact with the coil end turns and robustness to uneven coil geometries.

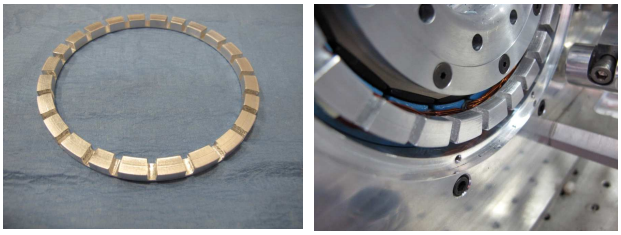

(A) (B)

Figure 11. PHOTOGRAPHS OF THE FLEXIBLE ALUMINUM INSERT (A) AND THE INSERT MOUNTED ON THE STATOR COILS (B).

Enhanced Design Performance

Stall current tests were performed at various levels to measure the heat transfer performance of the basic design. Currents ranging from $6A - 7.9A$ were applied. The $7.9A$ load is 8% higher than the continuous stall rating for the nominal motor design. The ambient temperature of the room was approximately $21°C$. Tests were performed with and without forced air. In this case a set of two cooling fans (combined power:$4W$, combined mass: $180g$) were used to cool the motor circumference.

The results are shown in Fig. 12. As the results show, the enhanced cooling design provides improved performance with reduced mass. The enhanced design increases the heat transfer coefficient from 1.25 to $1.51 W/K$ when no fans are used. When the PC fans are used, the heat transfer coefficient increases to $1.81 W/K$ which is comparable to the basic design under similar conditions. Substantial energy is saved when compared with the nominal case. For example, at $7.3A$, the enhanced design is projected to save $14.7W$ (13%) versus the nominal design. Comparing against the basic design, the enhanced design increases the torque density by $8\% - 13\%$ (depending on whether fans are used).

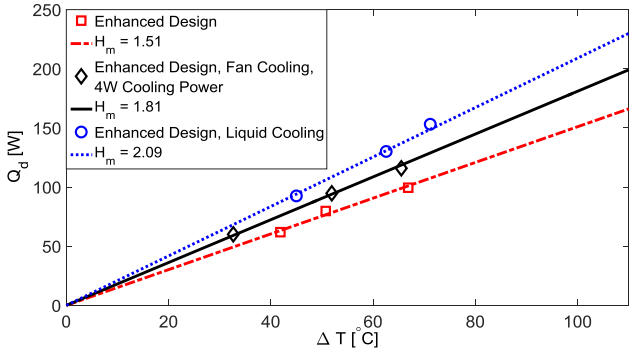

Figure 12. EXPERIMENTAL DATA FOR THE ENHANCED MOTOR DESIGN'S HEAT TRANSFER PERFORMANCE.

Liquid Cooling Performance

A liquid cooling test-bed was constructed consisting of a cooling jacket, a small liquid pump (TCS M400S, $34g$, $4.78 \times 10^{-5} m^3/s$), a PC radiator and fan, and a reservoir. The cooling jacket is slid directly over the stator and uses an O-ring on each end to contain the liquid. In this case, 39% of the stator's outer radial surface area is exposed to liquid. Despite this relatively small fraction, liquid cooling has a very large impact on performance. This system is illustrated in Fig. 13 and was not optimized for size or weight. The total mass of the components is $0.774kg$ and the breakdown of the masses is shown in Table 1. The combined power consumption from the pump and radiator fan is $2.5W$.

Liquid cooling performance was characterized using stall current tests at levels ranging from $6A - 9A$. The $9A$ command is 23% higher than the continuous stall rating of the nominal motor design. As the results in Fig. 12 show, the liquid cooling greatly improves heat transfer performance. The heat transfer coefficient of $2.09 W/K$ is 107% larger than that of the nominal design, and 15% better than the best performance with forced air. This means that the liquid cooled motor can provide 44% more continuous torque than the nominal design. From an efficiency standpoint, liquid cooling provides substantial benefit. With a $7.3A$ current, the motor and cooling system consume a combined $95.2W$. This is a $17.8W$ reduction when compared with the nominal design, and a $4.3W$ reduction when compared with the forced air case.

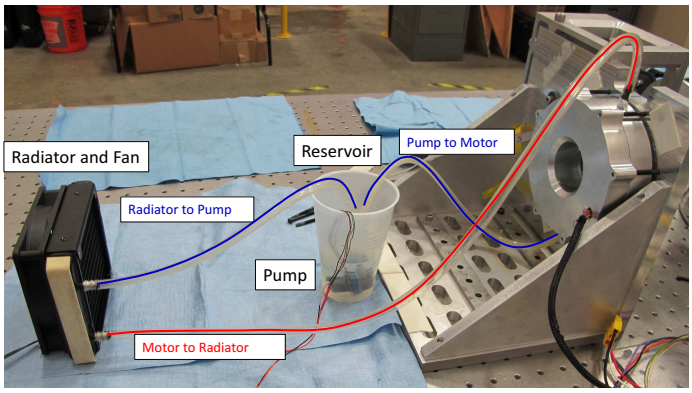

Figure 13. ILLUSTRATION OF THE LIQUID COOLING TEST-BED.

Table 1. MASS PROPERTIES FOR LIQUID COOLING COMPONENTS.

Item	Mass (kg)
Radiator and Fan	0.538
Tubing	0.0145
Jacket	0.0145
Pump	0.034
Reservoir	0.173

Best-Case Performance The best-case performance of the liquid-cooled motor can be predicted by idealizing the heat transfer with a two-resistor network. In this case, we assume the heat transfer through the radial liquid cooling dominates. A two resistor model can be created with r_1, representing the thermal resistance of the path from the coils to the outer layer of the back iron, and r_2 representing the thermal resistance of the path from the back iron to the environment. This simplified model is illustrated in Fig. 14. We can estimate the relative magnitudes of r_1 and r_2 by measuring the temperature of the back iron, T_I. We performed a liquid cooling experiment with a thermistor attached to the back iron. At steady state, the resulting temperatures were $T_{coil} = 92°C$, $T_I = 39°C$, and $T_a = 21°C$. These results demonstrate that during liquid cooling, r_2 has already been reduced to only 25% of the net thermal resistance. If r_2 was reduced to zero, the motor heat transfer coefficient, H_m, would be $2.8W/K$. This value represents a performance limit of our "minimally invasive" cooling techniques. Further improvements could be achieved through more complex solutions such as modifying the stator designs ([7]) or introducing additional cooling components such as chillers.

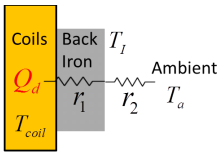

Figure 14. SCHEMATIC DIAGRAM OF THE SIMPLIFIED RADIAL HEAT TRANSFER MODEL.

Limiting Factors In these results, liquid cooling performance appears to be limited by the heat dissipation of the radiator. The reservoir water temperature increases substantially during an experimental trial. This illustrates that the heat from the motor is being transferred to the liquid, but this heat is not being fully removed in the radiator. A larger fluid reservoir provided improved performance during the 30 minute experimental trials, but we believe that the larger fluid volume simply takes longer to reach steady state conditions.

Corrosion Issues One potential issue with liquid cooling is the susceptibility of the back iron to corrosion. The results in this work used tap water which can be corrosive and therefore requires frequent removal of the cooling jacket and cleansing of the back iron. Two potential solutions to this are: 1) coating the back-iron layer with copper (provides good heat transfer and corrosion properties), or 2) using a cooling fluid with anti-corrosive additives. Note that the cooling fluid must be carefully selected to ensure safety at high temperatures.

DISCUSSION

The results of this work show how motor frame design and active cooling elements can substantially increase the heat transfer properties of high-torque DC motors. The enhanced heat transfer design not only provides increased torque density, but can also provide energetic improvements by reducing dissipated power. The enhanced design featuring tailored heat transfer solutions provides improved heat transfer, reduced weight, and design flexibility.

Design Tradeoffs

When using the housing design outlined in this work, choosing between passive cooling, forced air, and liquid cooling requires consideration of operating conditions, complexity, and size constraints. The passively cooled design proposed in this work provides a substantial improvement in heat transfer with no mass, power, or complexity penalty. Forced cooling through the use of small fans also provides little penalty in terms of mass (6% of total motor and housing mass) or complexity. This serves as a relatively simple way to achieve a 20% improvement in heat transfer and a 3% increase in torque density without significant

power or complexity costs. Torque density could be further optimized through more careful fan selection. The analysis in this work can be used to predict the energetic consequences of active cooling. At high operating currents, fans can provide a net energetic win, directly saving more energy than they consume by reducing motor resistance.

Liquid cooling provides superior heat transfer performance and enables increased continuous current levels. While the pump and radiator for liquid cooling do not require substantial power, the radiator and reservoir can be large and heavy. However, the radiator, reservoir, and pump can be used to cool multiple motors. Therefore, the size and weight penalties dramatically reduce if liquid cooling is used for multiple actuators in a system [4, 5]. In general, the inclusion of a circulatory system for liquid cooling represents a dramatic step change in the design of any particular mobile robotic system. Once the overhead of a liquid cooling system is integrated, it is likely beneficial to use it to aggressively cool as many motors as possible. On the other hand, the results presented herein indicate that a substantial fraction of the benefits may be gained with simpler alternatives.

Walking Robot Design

Our group has incorporated these lessons into a bipedal walking robot known as the Walking Anthropomorphic Novelly Driven Efficient Robot for Emergency Response (WANDERER). WANDERER is designed for high endurance walking performance for disaster response applications. The robot, shown in Fig. 15, incorporates the enhanced heat transfer design at all 12 of its leg joints. Currently WANDERER walks using relatively low power at the motors and therefore does not require liquid cooling. Passive cooling is used at $2/3$ of the leg motors and active cooling is used at the $1/3$ of the leg motors where power dissipation is especially high.

CONCLUSION

In this work we have shown how good heat transfer can increase the torque density and reduce the energy consumption of electromagnetic actuators for mobile robots. We have experimentally illustrated these benefits through a combination of housing design and the use of forced fluid flow (air and water). A lightweight and adaptable "enhanced cooling housing design" for frameless, high-torque motors has been outlined and experimentally validated. This design approach is compatible with a wide range of commercially available motors, and does not require modifications to the motor stator or rotor. Experimental results illustrate the improved heat transfer in ambient air, and fans or liquid cooling can quickly be added to further improve performance. Our group's latest bipedal robot features elements of the enhanced cooling design at all 12 of its leg actuators, resulting in increased torque capacity and reduced heating. In the future, this study could be extended to consider transient effects. A dynamic heat transfer model could be used to examine the role of improved heat transfer and active cooling on peak torque performance. This could enable dramatic one-time behaviors requiring very high momentary torques.

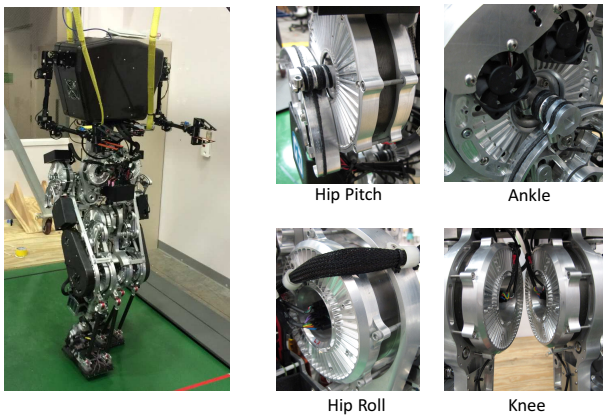

Figure 15. PHOTOGRAPHS OF THE WANDERER BIPEDAL ROBOT AND ITS HIGH HEAT TRANSFER MOTOR HOUSINGS.

ACKNOWLEDGMENT

The authors thank Timothy Blada and Kevin Dullea for their assistance with prototyping and testing.

This work was supported as part of DARPA's Maximum Mobility and Manipulation (M3) Program.

REFERENCES

[1] Hollerbach, J., Hunter, I., and Ballantyne, J., 1992. *A Comparative Analysis of Actuator Technologies for Robotics, The Robotics Review 2*. MIT Press, Cambridge, MA.

[2] Seok, S., Wang, A., Otten, D., and Kim, S., 2012. "Actuator design for high force proprioceptive control in fast legged locomotion". In Proc. of the IEEE/RSJ International Conference on Intelligent Robots and Systems, IEEE, pp. 1970–1975.

[3] Ruddy, B., 2012. "High Force Density Linear Permanent Magnet Motors: "Electromagnetic Muscle Actuators"". PhD Thesis, Massachusetts Institute of Technology, Cambridge, MA, October.

[4] Urata, J., Nakanishi, Y., Okada, K., and Inaba, M., 2010. "Design of high torque and high speed leg module for high power humanoid". In Proc. of the 2010 IEEE/RSJ International Conference on Intelligent Robots and Systems, IEEE, pp. 4497–4502.

[5] Urata, J., Hirose, T., Namiki, Y., Nakanishi, Y., Mizuuchi, I., and Inaba, M., 2008. "Thermal control of electrical motors for high-power humanoid robots". In Proc. of the 2008 IEEE/RSJ International Conference on Intelligent Robots and Systems, IEEE, pp. 2047–2052.

[6] Hochberg, U., Dietsche, A., and Dorer, K., 2013. "Evaporative cooling of actuators for humanoid robots". In Proc. of the IEEE/RAS International Conference on Humanoid Robots, Workshop on Humanoid Soccer Robots, IEEE, pp. 1–6.

[7] Liebman, A., 1998. "Thermally efficient linear motor analysis and design". MS Thesis, Massachusetts Institute of Technology, Cambridge, MA.

[8] Aghili, F., Hollerbach, J., and Buehler, M., 2007. "A Modular and High-Precision Motion Control System With an Integrated Motor". *IEEE/ASME Transactions on Mechatronics,* ***12***(3), June, pp. 317–329.

[9] Dauphinee, T., and Preston-Thomas, H., 1954. "A Copper Resistance Temperature Scale". *Review of Scientific Instruments,* ***25***(9), September, pp. 884–885.

[10] Gwinn, J., and Webb, R., 2003. "Performance and Testing of Thermal Interface Materials". *Microelectronics Journal,* ***34***(3), March, pp. 215–222.